What determines the reconnection rate at the dayside magnetosphere?

Joseph E. Borovsky,[1] Michael Hesse,[2] Joachim Birn,[1] and Maria M. Kuznetsova[2]

Received 16 July 2007; revised 1 December 2007; accepted 27 March 2008; published 19 July 2008.

[1] Reconnection between the magnetosphere and magnetosheath at the dayside magnetopause is studied for southward IMF using high-resolution 3-D MHD simulations. The BATSRUS code is run at CCMC with a resistive spot added on the magnetopause to ensure that fast reconnection occurs and to control the reconnection physics. A large range of Mach numbers (1.9–15) are run. The reconnection rate at the nose of the magnetosphere is measured and compared with local plasma parameters and with upstream-solar wind parameters. It is found that the reconnection rate is controlled by four local plasma parameters: B_s (the magnetic field strength in the magnetosheath), B_m (the magnetic field strength in the magnetosphere), ρ_s (the plasma mass density in the magnetosheath), and ρ_m (the plasma mass density in the magnetosphere). The Cassak-Shay formula for fast reconnection was tested and found to successfully describe the reconnection rate on the dayside magnetopause. It was found that reconnection itself does not significantly modify the local plasma parameters that control dayside reconnection and argued that reconnection does not significantly alter the flow pattern of the magnetosheath. This means that dayside reconnection is not "driven" in the sense that plasma pileup occurs to change the local parameters to adjust the reconnection rate to balance the driving. A "plasmasphere effect" was observed in the simulations wherein high-density magnetospheric plasma flows into the magnetopause reconnection site and mass loads the reconnection: a spatially localized plume of plasma was observed to locally reduce the reconnection rate by about a factor of 2.

Citation: Borovsky, J. E., M. Hesse, J. Birn, and M. M. Kuznetsova (2008), What determines the reconnection rate at the dayside magnetosphere?, *J. Geophys. Res.*, *113*, A07210, doi:10.1029/2007JA012645.

1. Introduction

[2] When two different plasmas are in contact, they may undergo magnetic field-line reconnection (magnetic merging). For fast Petschek-type reconnection [*Petschek*, 1964; *Sonnerup*, 1970], the magnetic field lines change their topologies along a merging line. The rate of reconnection can be defined as the inflow velocity of plasma into the merging line [e.g., *Parker*, 1979; *Birn and Priest*, 2007]. Equivalently, the rate of reconnection can be defined as the strength of an electric field parallel to the merging line [e.g., *Sonnerup*, 1979; *Vasyliunas*, 1984; *Schindler et al.*, 1988].

[3] The idealized case of the reconnection between two identical plasmas with antiparallel magnetic fields has been extensively studied. In this geometry, when fast (Petschek) reconnection occurs the reconnection rate is governed by the Alfven speed v_A in the inflowing plasma, with the inflow velocity of plasma into the reconnection site being $v_{in} \approx 0.1\ v_A$ [*Parker*, 1973a; *Birn et al.*, 2001]. The reconnection rate (amount of magnetic flux reconnecting per unit time per unit length of the reconnection line) is then $R = v_{in}B_{in} \approx 0.1\ v_A B$, where v_A and B are the Alfven speed and magnetic field strength in the ambient plasma. (The quantity R is also equivalent to the strength of an electric field along the merging line.) The 0.1 factor is a property of the geometry of the reconnection: it is the ratio of the angular widths of the outflow to inflow regions. Computer simulations utilizing particle-in-cell [*Hesse et al.*, 2001; *Pritchett*, 2001], hybrid [*Shay et al.*, 1999; *Kuznetsova et al.*, 2001], and 3Hall-MHD [*Shay et al.*, 2001; *Huba and Rudakov*, 2004] methods obtain this rate of $\sim 0.1\ v_A B$ [see *Birn et al.*, 2001]. Resistive-MHD simulations also obtain this rate (1) if spatially localized strong resistivity is imposed between the two plasmas [*Ugai and Tsuda*, 1977; *Yan et al.*, 1992; *Birn and Hesse*, 2001; *Borovsky and Hesse*, 2007; *Birn et al.*, 2008] or (2) if current-dependent resistivity is used to allow the fast reconnection to proceed [*Otto*, 2001]. Resistive-MHD with uniform resistivity or with only numerical resistivity tends to obtain a reconnection rate that depends on the value of the resistivity and tends to form long Sweet-Parker reconnection layers [cf. *Birn and Hesse*, 2001; *Dorelli et al.*, 2004] rather than the Petschek reconnection spot.

[4] When the two reconnecting plasmas are not identical, or when the magnetic fields of the two plasmas are not exactly antiparallel, then the reconnection rate is no longer simply $0.1\ v_A B$. When the magnetic field directions in two

[1]Space Science and Applications Group, Los Alamos National Laboratory, Los Alamos, New Mexico, USA.
[2]Space Weather Laboratory, NASA/Goddard Space Flight Center, Greenbelt, Maryland, USA.

Copyright 2008 by the American Geophysical Union.
0148-0227/08/2007JA012645

symmetric plasmas form an angle of θ with respect to each other ($\theta = 0°$ being parallel and $\theta = 180°$ being antiparallel), *Sonnerup* [1974] theoretically demonstrated that the MHD reconnection rate would scale as $v_A B\sin(\theta/2)$ [see also *Russell and Atkinson*, 1973; *Pritchett and Coroniti*, 2004; *Huba*, 2005; *Swisdak et al.*, 2005]. For antiparallel reconnection between plasmas with different mass densities ρ, *Borovsky and Hesse* [2007] using resistive-spot compressive-MHD simulations found the reconnection rate to be approximately 0.1 $v_{Ah}B$, where $v_{Ah} = B/(0.5\ \mu_o\rho_1 + 0.5\ \mu_o\rho_1)^{1/2}$ is a hybrid Alfven speed that depends on the mass densities ρ_1 and ρ_2 of both inflowing plasmas. For antiparallel reconnection between plasmas with different magnetic field strengths B and different mass densities ρ, *Cassak and Shay* [2007] derived an expression for the reconnection rate, which is

$$R = CS, \tag{1}$$

where C is a coefficient ($C \sim 0.1$) that depends of the geometry of the reconnection process (opening angle of outflow divided by opening angle of inflow) and where the function S is given by

$$S = 2(B_1B_2)^{3/2}(\mu_o\rho_1B_2 + \mu_o\rho_2B_1)^{-1/2}(B_1 + B_2)^{-1/2}. \tag{2}$$

The function S is a hybrid Alfven speed multiplied by a hybrid magnetic field strength. In this paper we will denote $S(B_1, B_2, \rho_1, \rho_2)$ as the "Cassak-Shay function". Expressions (1) and (2) can be found in equations (16), (17), and (18) of *Cassak and Shay* [2007], with $C \equiv \delta/L$ being the reconnection "aspect ratio".

[5] Reconnection between the dayside magnetospheric plasma and the magnetosheath plasma is of particular importance because this dayside reconnection is believed to control the energy input into the magnetosphere from the solar wind [e.g., *Dungey*, 1961; *Hones*, 1984; *Kamide and Slavin*, 1986; *Goertz et al.*, 1993; *Russell*, 2000; *Cowley et al.*, 2003] and hence the rate of convection in the magnetosphere.

[6] The important question arises: What controls the local reconnection rate? There are several possible answers. Is it the vB_z value of the solar wind driving reconnection? Is it some local hybrid Alfven speed of the magnetosheath and magnetospheric plasmas inflowing into the reconnection site? Or can it be both? Finally, can magnetospheric plasma affect the reconnection rate?

[7] In this report the control of the local reconnection rate at the dayside magnetopause between the magnetosphere and magnetosheath will be studied by means of computer simulations. Other issues that are being studied separately are (1) what controls the total reconnection rate at the dayside magnetopause, which is a product of the local reconnection rate and the length of the merging line, (2) how the total reconnection rate corresponds to ionospheric and magnetospheric potentials, and (3) whether ionospheric-conductivity effects (polar-cap saturation) can affect the reconnection rate.

[8] In this report high-resolution 3-dimensional MHD simulations of the solar wind-driven magnetosphere are run to study dayside reconnection. Special care is taken to ensure that the simulation code obtains the correct amount of magnetopause reconnection. Only steady reconnection in the equatorial plane for a nontilted dipole under steady southward IMF is investigated. According to the simulations of *Raeder* [2006], for the nontilted-dipole simulations performed here transient reconnection should not occur. Investigating when and where dayside reconnection is steady versus transient [cf. *Russell et al.*, 1997; *Rodger et al.*, 2000; *Trattner et al.*, 2005; *Birn and Priest*, 2007] is beyond the scope of the present numerical simulations.

[9] This manuscript is organized as follows. In section 2 the computer simulations used to investigate the reconnection at the dayside of the magnetosphere are explained. In section 3 the reconnection rates measured in the simulations are discussed. In section 4 the parameters controlling the rate of reconnection are determined. In section 5 the "plasmasphere effect" (the effect of magnetospheric plasma density on the rate of dayside reconnection) is elaborated upon. Section 6 contains a summary and discussion about local control of dayside reconnection, plasma pileup at the nose of the magnetosphere, errors in measuring and simulating dayside reconnection, and future work that is needed.

2. Computer Simulations

[10] To discern what determines the rate of reconnection at the dayside magnetopause using computer simulations, the simulations must be three dimensional, well resolved, able to support Petschek reconnection, and with numerical diffusivity under control. To satisfy this, the BATSRUS three-dimensional MHD simulation code [*Powell et al.*, 1999; *Gombosi et al.*, 2000; *De Zeeuw et al.*, 2000] is run with a high-resolution grid, with the low-diffusivity Sokolov numerical scheme, and with an added localized resistivity that is larger than numerical resistivity. The highest-resolution gridding is $\Delta X = \Delta Y = \Delta Z = 1/16\ R_E$: in Simulation A this $1/16\ R_E$ gridding extends from $X = 6\ R_E$ to $X = 12\ R_E$ and $Z = -4.5\ R_E$ to $Z = 4.5\ R_E$ at the nose and is wrapped around in Y to the terminator, and in Simulation B this $1/16\ R_E$ gridding extends from $X = 6\ R_E$ to $X = 13.5\ R_E$ and $Z = -4.5\ R_E$ to $Z = 4.5\ R_E$ at the nose and is wrapped around in Y to the terminator.

[11] The MHD simulations are run with a simple solar wind and a simple ionospheric model. Two large simulations are run: the parameters of the two runs are listed in Table 1. Simulation A is a high-Mach-number run (M_{ms} = 7.5 – 15) and Simulation B is a low-Mach-number run (M_{ms} = 1.9–4.4). The inner boundary of the MHD calculation is a sphere of radius $2.5\ R_E$ with a fixed cold-plasma density of 28 cm^{-3} at the boundary [*Ridley et al.*, 2004]. The northern and southern ionospheres are taken to have uniform height-integrated Pedersen conductivities of 5 mho and height-integrated Hall conductivities of 0. The solar wind velocity is steady or slowly varying in the simulations, straight onto a nontilted dipole. The solar wind magnetic field is steady and due southward. The solar wind is relatively cool with T = 50,000 °K. When the solar wind is varied, only v is varied. Note that owing to the large CPU resources need for each high-resolution run, the full range of interesting solar wind parameters have not been explored, particularly magnetic field orientations that are not exactly southward.

Table 1. Parameters of the Two Major Simulations Employed in the Dayside-Reconnection Study[a]

		Simulation A	Simulation B
Dipole tilt	θ	none	none
Solar wind speed	v_x	−400 to −800 km/s	−300 to −700 km/s
Solar wind east-west velocity	v_y	0	0
Solar wind north-south velocity	v_z	0	0
Solar wind number density	n	5 cm^{-3}	2 cm^{-3}
Solar wind radial magnetic field strength	B_x	0	0
Solar wind east-west magnetic field strength	B_y	0	0
Solar wind north-south magnetic field strength	B_z	−5 nT	−10 nT
Solar wind temperature	T	50,000°K	50,000°K
Solar wind ram pressure	ρv^2	1.33–5.34 nPa	0.3–1.6 nPa
Solar wind electric field	E_y	2–4 mV/m	3–7 mV/m
Alfven speed in solar wind	v_A	49.2 km/s	156 km/s
Acoustic speed in solar wind	C_s	20.3 km/s	20.3 km/s
Magnetosonic speed in solar wind	C_{ms}	53.2 km/s	157 km/s
Magnetosonic Mach number of solar wind	M_{ms}	7.5–15	1.9–4.4
Height-integrated Pedersen conductivity of ionospheres	Σ_P	5 mho	5 mho
Height-integrated Hall conductivity of ionospheres	Σ_H	0	0
Maximum resistivity of spot	η	1.26×10^5 Ω-m	1.26×10^5 Ω-m
Simulation-box limit	X_{max}	33 R_E	33 R_E
Simulation-box limit	X_{min}	−255 R_E	−255 R_E
Simulation-box limit	Y_{max}	48 R_E	48 R_E
Simulation-box limit	Y_{min}	−48 R_E	−48 R_E
Simulation-box limit	Z_{max}	48 R_E	48 R_E
Simulation-box limit	Z_{min}	−48 R_E	−48 R_E

[a]Simulation A is high Mach number and Simulation B is low Mach number.

[12] To enable fast reconnection to occur (instead of a Sweet-Parker layer), a localized region ("spot") of high resistvity is added to the nose of the magnetosphere. The GEM Reconnection Challenge [*Birn et al.*, 2001] established that MHD simulations can obtain the correct reconnection rate if a resistive spot is used, providing that the resistivity of the spot is high enough [see also *Birn et al.*, 2008]. To get the reconnection rate correct, there is a further restriction on the spatial size of the spot. The requirements for the value of the resistivity and for the size of the spot are discussed in the Appendix A. The spot is centered on the B_z reversal at the magnetopause (northward in the magnetosphere and southward in the magnetosheath) and the spot is moved as the reversal location moves. The X location of the B_z reversal is denoted as $X_o(Y, Z)$. This resistive spot is shown in the two panels of Figure 1: the left panel is a Z-versus-x cut at Y = 0 (noon-midnight meridianal plane) and the right panel is a Y-versus-X cut at Z = 0 (equatorial plane). The spot is narrow in the X direction, longer in the Z direction, and even longer in the Y direction. The resistivity of the spot has a hyperbolic-secant profile as a function of X, Y, and Z, which is

$$\eta = 1.26 \times 10^5 \text{ ohm-m } \operatorname{sech}((X - X_o)/L_x)\operatorname{sech}(Y/L_y) \cdot \operatorname{sech}(Z/L_z), \quad (3)$$

where $L_x = 1/8\ R_E$, $L_y = 4\ R_E$, and $L_z = 1\ R_E$. Note that the peak resistivity of 1.26×10^5 ohm-m corresponds to a peak magnetic diffusivity of $\eta/\mu_o = 1 \times 10^{11}\ m^2/s$. The value of X_o is determined as follows during a simulation. At every value of Y and Z, the B_z value as a function of X is surveyed, the location in X of the B_z reversal on the dayside is determined, and X_o is assigned to this X location.

[13] Figure 2 shows Y = 0 cuts of the plasma flow velocity in the dayside region of the two major simulations: the left panel is from Simulations A (high Mach numbers) and the right panel is from Simulation B (low Mach numbers). The color indicates the plasma flow speed, red being fastest and blue being near zero. Magnetic field lines are indicated in the two figures: red field lines have both foot points on the Earth, black field lines have one foot point on the Earth and one in the solar wind, and blue field lines have both foot points in the solar wind. The arrow heads indicate the direction of the magnetic field. In the left panel the solar wind and magnetosheath are clearly seen, as are the two outflow jets from the dayside reconnection site at (X, Z) ≈ (8.5, 0). In the right panel the two reconnection flow jets from the reconnection site at (X, Z) ≈ (11.5, 0) are clearly seen but the bow shock separating the solar wind and magnetosheath is located outside the figure (at X ≈ 24 R_E).

[14] In Figure 3 the plasma flow streamlines in the Y = 0 plane are shown from Simulation A. In this figure, the color represents the local value of B_z. The reversal between B_z positive (northward) and B_z negative (southward) is in the light-blue color band. The reconnection site (field reversal) is located at (X, Y) = (9.15, 0). Note that, as is usual for Petschek fast reconnection, most streamlines do not go through the reconnection site but rather plasma joins into the fast outflow jets owing to the action of the newly reconnected magnetic field (i.e., via $\mathbf{j} \times \mathbf{B}$ acceleration away from the reconnection site). Simulation B (low Mach number) shows essentially the same properties.

[15] Figure 4 shows the plasma flow streamlines in the equatorial plane Z = 0 in Simulation A. Here the color represents the value of B_z. The arrow heads represent the local direction of flow in the z = 0 plane. Note that the plasma flow in the magnetosphere is focused toward the nose of the magnetosphere at (X, Y) = (9.15, 0) whereas the plasma flow in the magnetosheath is diverging away from the nose. Simulation B (low Mach number) shows essentially the same properties.

[16] Figure 5 shows several plasma parameters plotted along the sun-Earth line y = 0 and z = 0 through the

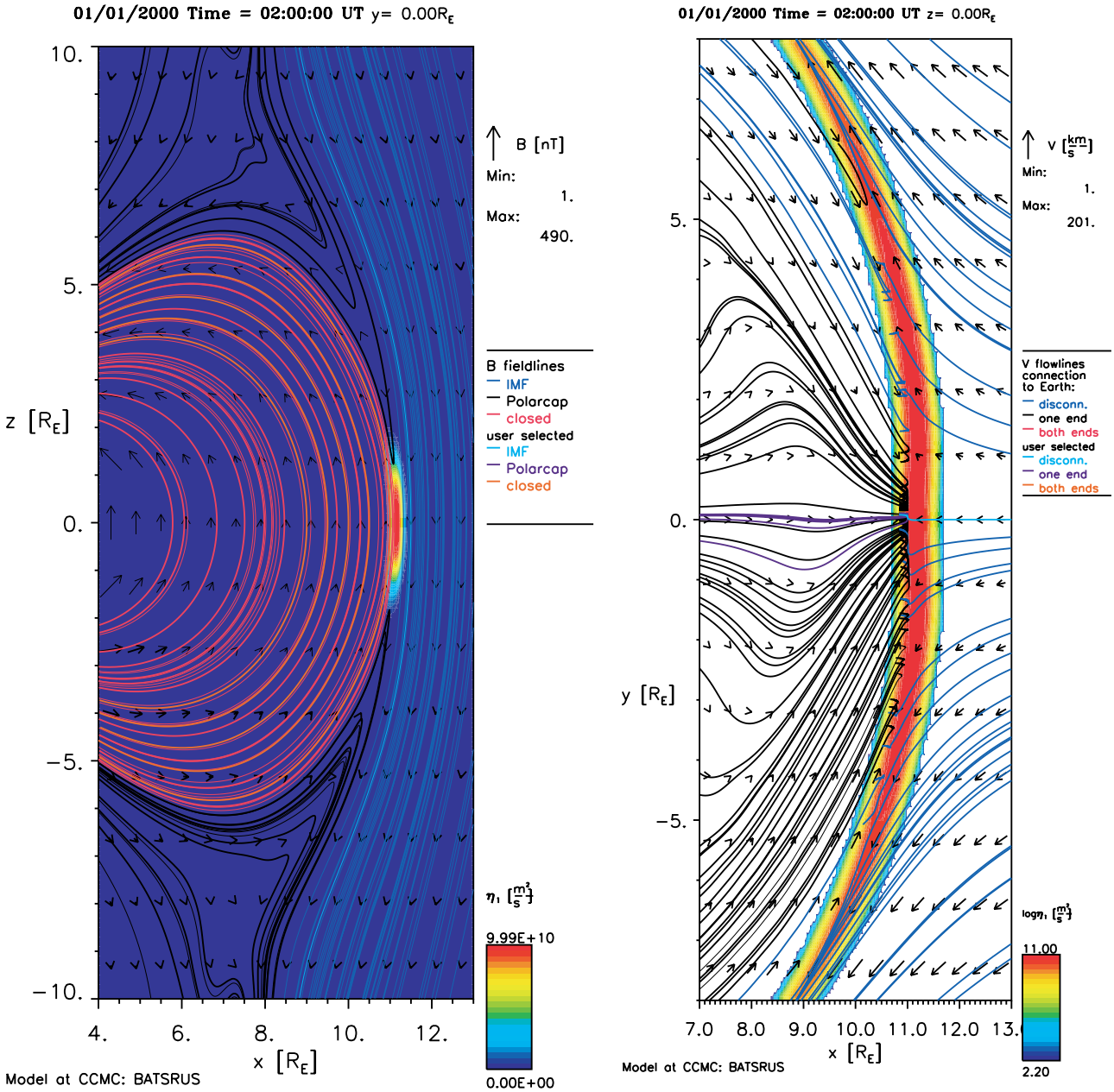

Figure 1. Resistive spot (color) added to the BATSRUS simulation code is shown in a noon-midnight cut (left) and in the equatorial plane (right). In the left magnetic field lines are indicated and in the right flow streamlines are indicated.

reconnection site at the nose of the magnetosphere. The top panel is from Simulation A when the solar wind speed is 600 km/s and the bottom panel is from Simulation B when the solar wind speed is 300 km/s. Looking at the curves for $|B_z|$ (red), the various regions of the simulation can be seen. In the top panel at the right end is the solar wind with $B_z = -5$ nT. Moving to the left the magnetic field strength jumps up by a factor of 4 across the high-Mach-number ($M_{ms} \approx 11.3$) bow shock. B_z increases by a further factor of about 2 in the magnetosheath between the shock and the magnetopause. At the magnetopause (X = 9.33) the magnetic field strength goes through a minimum as B_z reverses sign. Finally, in the magnetosphere B_z increases as r^{-3} moving to toward the left in the dipolar region. In the solar wind and magnetosheath a similar behavior is seen for the plasma density n (blue curves in Figure 5), except that the increase through the magnetosheath is weaker for n than it is for B_z (owing to the divergence of the magnetosheath flow away from the nose in the y and z directions, which decreases the scalar n more than it decreases the vector **B**). The current density j is plotted in green along the Sun-Earth line in Figure 5; note the bow shock and the magnetopause. Owing to the intense resistivity of the spot on the magnetopause (plotted in gray), the current density is double peaked on the sides of the spot. This double current has been seen in prior resistive-spot MHD simulations. Also plotted in black in Figure 5 is the absolute value of the x component of the plasma flow velocity $|v_x|$ along the Sun-Earth line. As can be seen, v_x

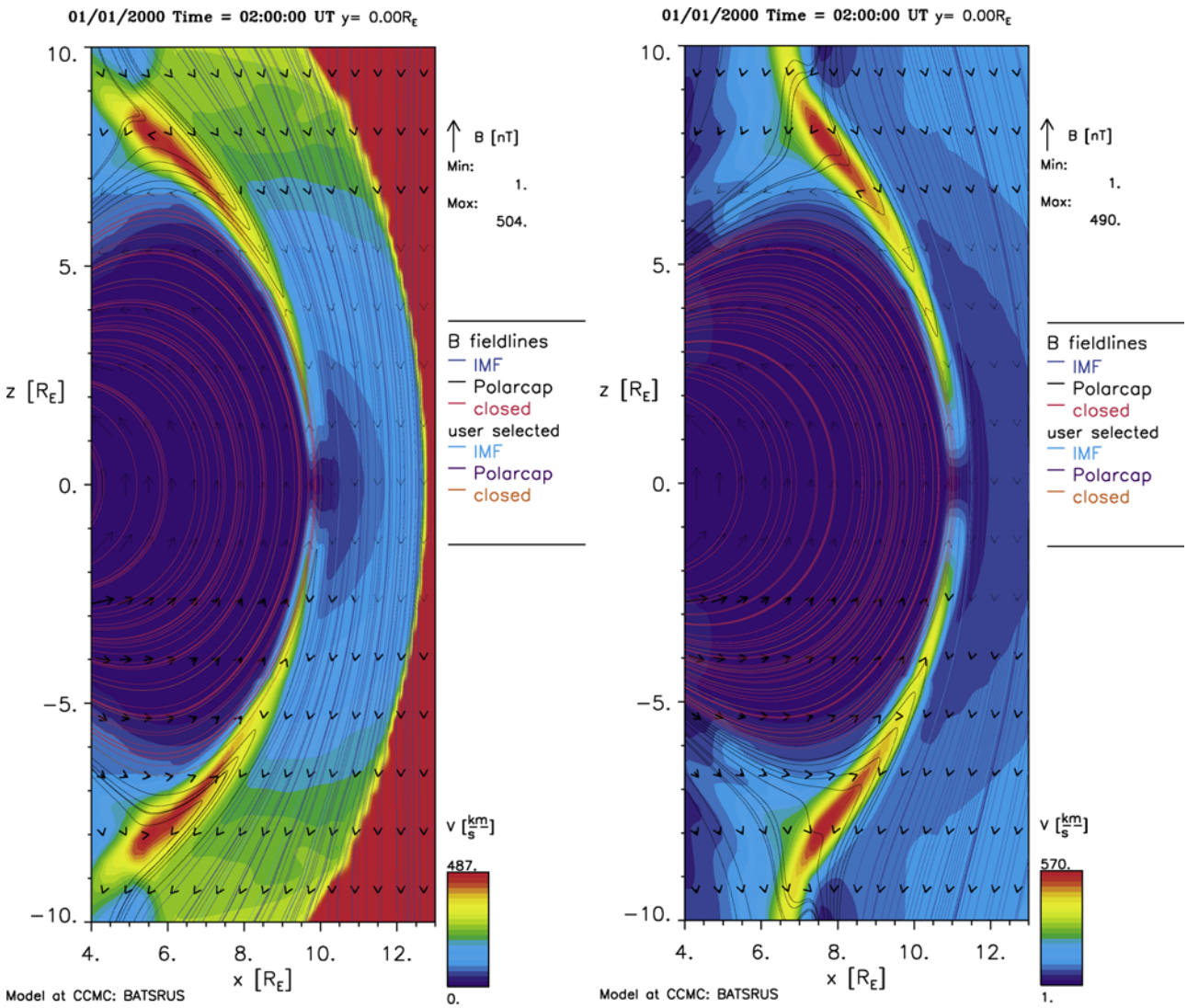

Figure 2. Overviews of reconnection in the dayside magnetosphere are shown in these two noon-midnight meridianal cuts: the left is from Simulation A (high Mach number) and the right is from Simulation B (low Mach number). The color is the plasma flow speed. Note the two jets of flow emanating upward and downward from the nose reconnection sites in both panels.

drops by a factor of 4 across the high-Mach-number bow shock, then drops further across the magnetosheath from the bow shock to the magnetopause. The flow velocity v_x goes through zero at the reconnection site and is positive in the magnetosphere. Note that the bow shock is much further out in the low-Mach-number simulation (bottom panel) than in the high-Mach-number simulation (top panel).

3. Reconnection Rate

[17] In the top panel of Figure 6 the magnetic-flux transport v_xB_z is plotted in red along the Sun-Earth line at a time in Simulation A when the solar wind velocity is 400 km/s. The magnetic-flux transport has a value of 2000 nT km/s in the solar wind, which corresponds to a duskward electric field of 2×10^{-3} V/m. This v_xB_z value decreases by about a factor of 2 in the magnetosheath from the bow shock to the nose of the magnetosphere owing to the divergence of the magnetosheath flow away from the nose of the magnetosphere. The y-component electric field E_y along the Sun-Earth line is given by $E_y = v_xB_z + \eta j_y$; this electric field is plotted in black in Figure 6 and ηj_y is plotted in green.

[18] The reconnection rate R at the nose of the magnetosphere is measured by evaluating ηj_y at the magnetic field reversal in the magnetopause.

[19] The Cassak-Shay function S (expression (2)) is also be evaluated at the nose of the magnetosphere. For this formula, B and n on the magnetosheath side are evaluated where their smooth trends in the magnetosheath begin to steepen near the reconnection site, and likewise B and n on the magnetospheric side are evaluated where their smooth trends in the magnetosphere begin to steepen near the reconnection site. In the plots of Figure 6, these points are approximately the points where $|v_xB_z|$ begins to rapidly decline in magnitude on either side of the reconnection site.

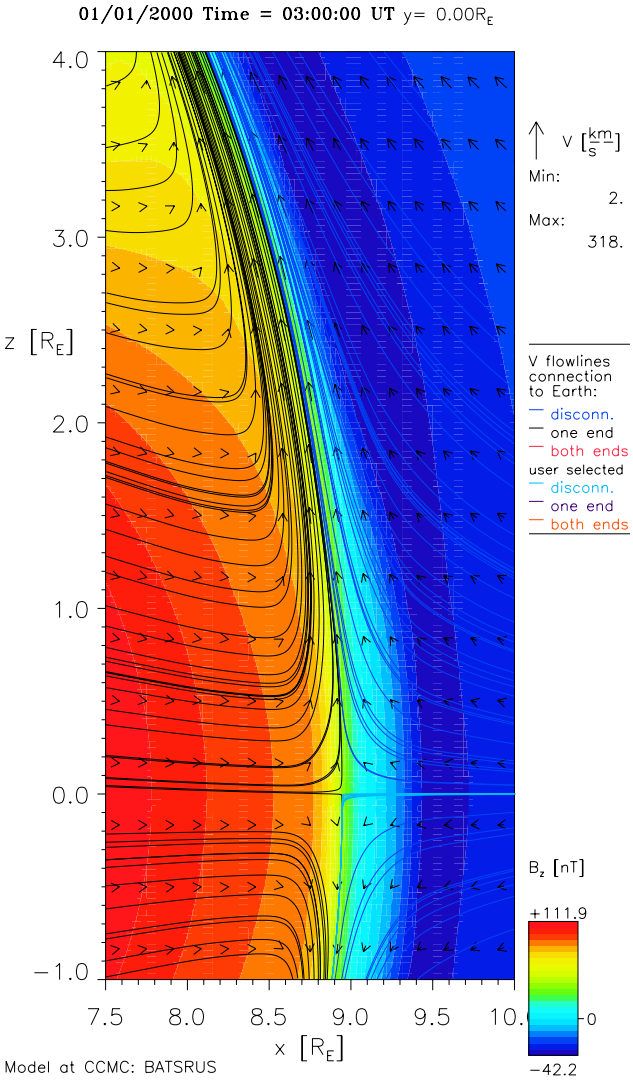

Figure 3. Plasma flow streamlines are shown in the noon-midnight meridianal plane for Simulation A. The color represents B_z, with green to red being positive and dark blue being negative.

[20] In Figure 7 the solar wind parameters are plotted as a function of time in Simulation A (top) and B (bottom). The solar wind velocity is plotted in green, the solar wind magnetic field strength is plotted in blue, and the solar wind number density is plotted in red. The solar wind velocity is constant at 400 km/s for 85 min, then it is slowly ramped up. At approximately every 5 min the reconnection rate at the nose is measured in the simulations. The measured reconnection rates are plotted as functions of time (black curves) in Figure 7. As can be seen as the solar wind velocity increases, the rate of reconnection increases.

[21] In the two panels of Figure 8 the local plasma parameters at the nose of the magnetosphere are plotted as functions of time from Simulation A (top panel) and Simulation B (bottom panel), as is the measured reconnection rate R. As can be seen, R responds to a combination of the local plasma parameters: R increases when B_m and/or B_s increase, and R decreases when ρ_m increases.

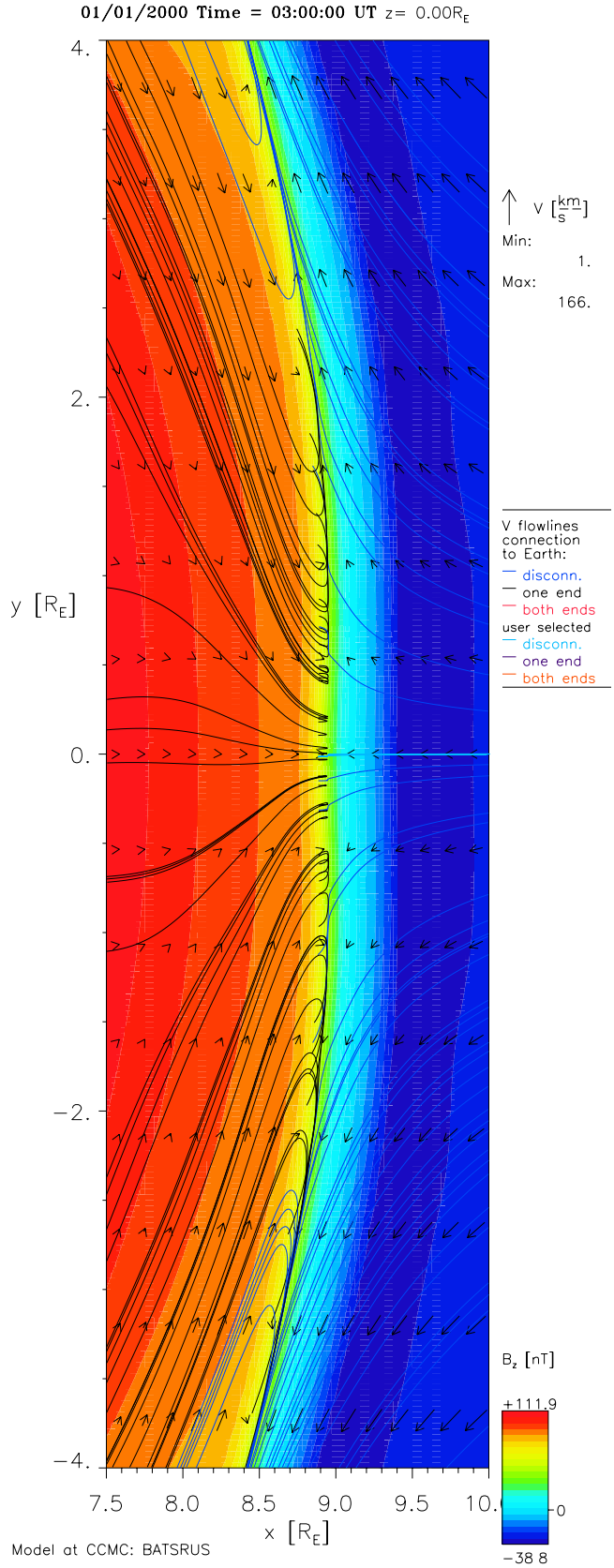

Figure 4. Plasma flow streamlines are shown in the equatorial plane for Simulation A. The color represents B_z, with green to red being positive and dark blue being negative.

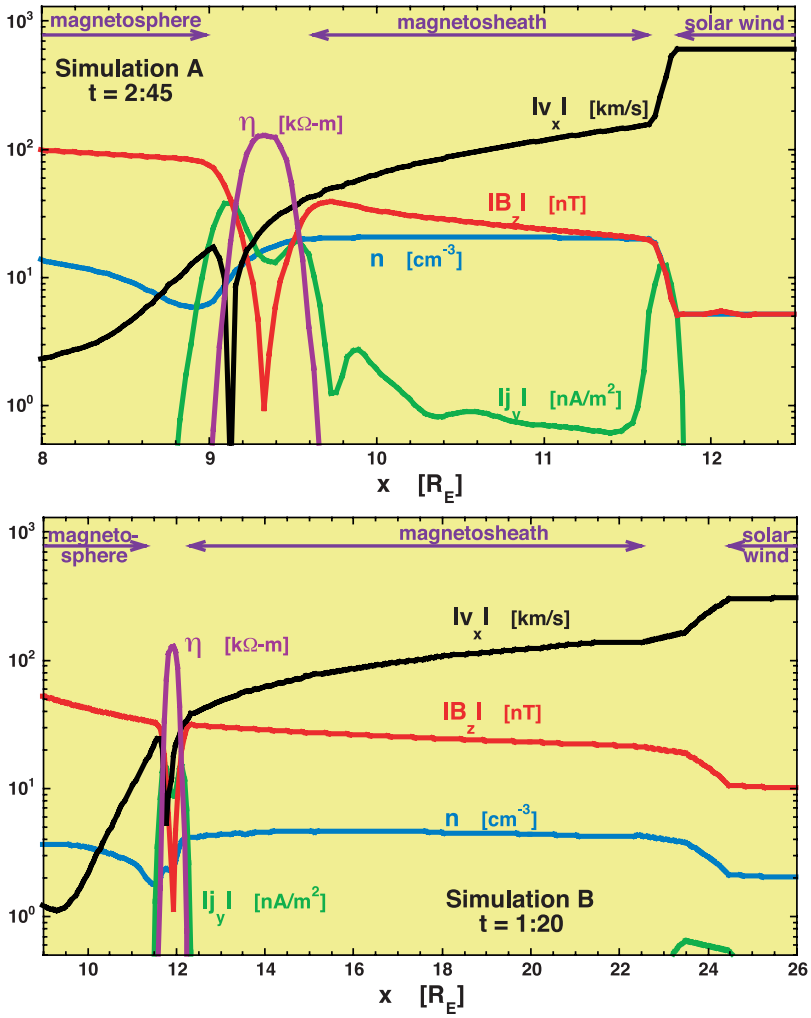

Figure 5. For Simulation A (top) and Simulation B (bottom) several parameters (magnitude of the X flow velocity $|v_x|$, magnitude of the magnetic field strength $|B_z|$, plasma number density n, resistivity η, and magnitude of the Y-direction current density $|j_y|$) are plotted as functions of X along the Sun-Earth line. At the top of each panel the location of the solar wind, magnetosheath, and magnetosphere are indicated. Note that the X scale is very different for the two panels: at low Mach numbers (bottom) the magnetosheath extends out much further around the magnetosphere.

[22] In Figure 9 the measured reconnection rate R, the solar wind electric field $(v_xB_z)_{sw}$, and the Cassak-Shay function S are plotted as functions of time for Simulation A (solid points) and Simulation B (hollow points). The units of all three quantities are nT km/s (which are the same as gauss cm/s). As can be seen in Figure 9, the behavior of the measured reconnection rate R follows more closely the behavior of the Cassak-Shay function S than it does the solar wind electric field $(v_xB_z)_{sw}$.

[23] In Figure 10 the reconnection rate R divided by the Cassak-Shay function S and the reconnection rate R divided by the upstream solar wind electric field $(v_xB_z)_{sw}$ are plotted as functions of time for simulation A (solid points) and simulation B (hollow points). As can be seen, R is much better described as a constant times S than it is as a constant times $(v_xB_z)_{sw}$. For the two simulations A and B, the ratio R/S varies by 18% (standard deviation over mean) where the average value of R/S is 0.11. Hence in expression (1) the constant C should be taken to be $C \approx 0.11$.

4. Parameters Controlling the Reconnection Rate

[24] It was concluded in Section 3 that the Cassak-Shay formula (expressions (1) and (2)) describes the rate of reconnection at the nose of the magnetosphere. Using the subscripts "m" for magnetosphere and "s" for magnetosheath, and taking $C \approx 0.1$, expressions (1) and (2) are rewritten to yield

$$R = 0.1\ \mu_o^{-1/2} B_s^{3/2} B_m^{3/2} / \left[(B_s \rho_{rm} + B_m \rho_s)^{1/2} (B_s + B_m)^{1/2} \right]. \quad (4)$$

According to expression (4), the reconnection rate is a function of four variables: B_m, ρ_m, B_s, and ρ_s. These four parameters and the reconnection rate R are coupled at the nose of the magnetosphere.

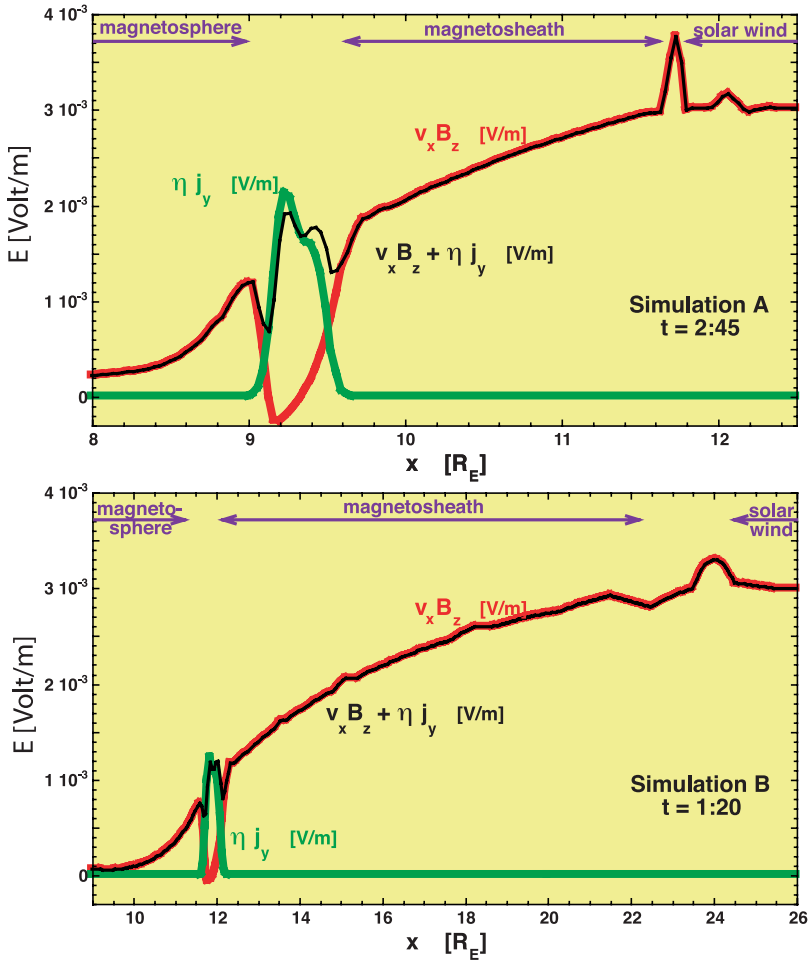

Figure 6. For Simulation A (top) and Simulation B (bottom) the Y component of the convection electric field v_xB_z (red), the Y component of the resistive electric field ηj_y (green), and the Y component of the total electric field $v_xB_z + \eta j_y$ (black) are plotted as functions of X along the Sun-Earth line. At the top of each panel the location of the solar wind, magnetosheath, and magnetosphere are indicated.

[25] Knowing that the Cassak-Shay formula (4) holds, which describes the reconnection rate in terms of local plasma parameters, two scenarios are possible: (1) driving determines the reconnection rate and the local plasma parameters follow or (2) the local plasma parameters determine the reconnection rate and reconnection is not driven. In Scenario 1 v_xB_z of the solar wind determines the rate of reconnection and magnetosheath plasma may pile up at the nose of the magnetosphere to change B_s and ρ_s to adjust the right-hand side of expression (4) to match the driving rate of reconnection. In Scenario 2 the reconnection rate R is governed by the right-hand side of expression (4) and the magnetosheath-side inflow velocity v_{xs} varies so that $R = v_{xs}B_{zs}$ agrees with the right-hand side of expression (4). In both scenarios the solar wind has (some) control of the reconnection rate, but differently: in Scenario 1 v_xB_z of the solar wind directly sets the reconnection rate and in Scenario 2 the solar wind parameters determine the properties of the bow shock and magnetosheath flow profile which in turn determine the reconnection rate. We would like to know which scenario is most accurate: i.e., which picture provides the best description and most insight.

[26] Scenario 2 holds if reconnection itself does not modify the parameters (B_m, ρ_m, B_s, and ρ_s) going into the right-hand side of expression (4). To check the notion that the rate of reconnection does not strongly affect B_m, ρ_m, B_s, and ρ_s, pairs of MHD simulations with purely northward IMF and purely southward IMF are compared: in the northward-IMF simulations dayside reconnection is off and in the southward-IMF simulations dayside reconnection is on. Two such pairs of simulation are examined in the two panels of Figure 11. The top panel is a low-Mach-number pair (M_{ms} = 1.9) and the bottom panel is a high-Mach-number pair (M_{ms} = 6.3). The magnetic field strength B, plasma number density n, and plasma entropy density S (= $P/n^{5/3}$) are plotted in the solar wind and magnetosheath. The plotting does not extend into the boundary layer: when the entropy density of the plasma begins to change, the plotting terminates. (These termination points are the points used to evaluate the Cassak-Shay formula.) Note the plasma depletion layers [*Zwan and Wolf*, 1976] in Figure 11 in the magnetosheath near the magnetopause where the field strength increases and the plasma density decreases. Plasma depletion layers are commonly seen experimentally [e.g., *Song et al.*, 1990; *Anderson and Fuselier*, 1993; *Phan and*

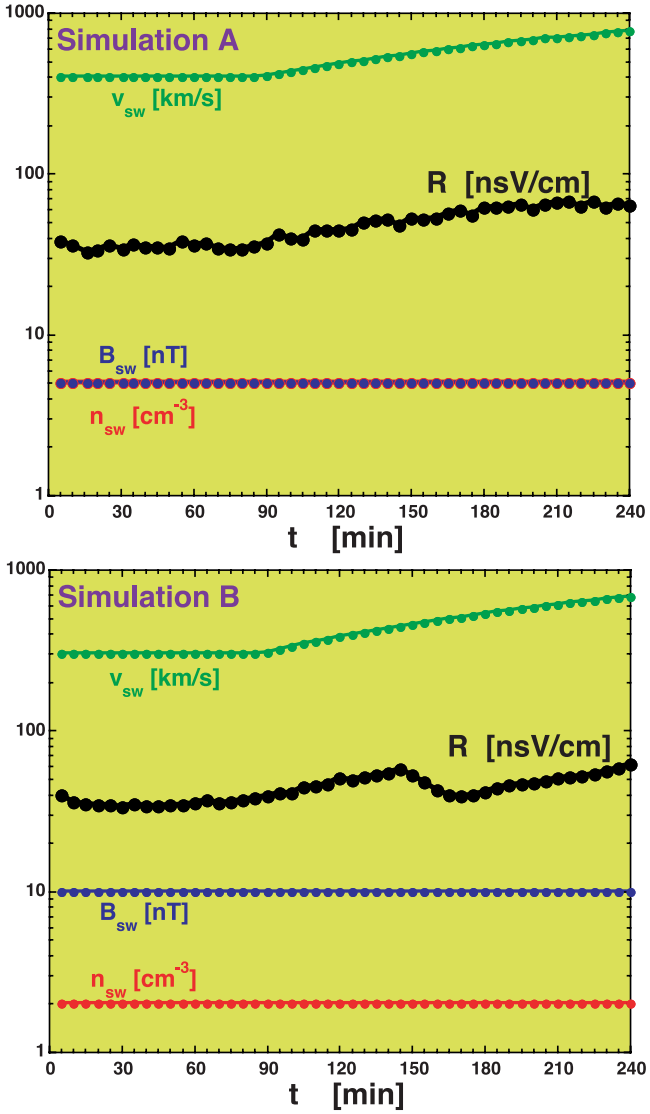

Figure 7. For Simulation A (top) and Simulation B (bottom), the solar wind velocity (green), solar wind magnetic field strength (blue), solar wind density (red), and measured reconnection rate at the nose (black) are plotted as functions of time every 5 min. (The units of R are nano statVolts per centimeter.)

Paschmann, 1995] and in global MHD simulations [e.g., *Wu*, 1992; *Siscoe et al.*, 2002; *Wang et al.*, 2004]. Note also that the northward-IMF depletion layer in the high-Mach-number case (lower panel) is weaker than the northward-IMF depletion layer in the low-Mach-number case (top panel); this is probably owed to the fact that at high Mach number the plasma β is high in the magnetosheath and the flow is more akin to gasdynamics than is the case for low Mach number with a low-β magnetosheath. As can be seen in the two panels of Figure 11, in both of these cases ρ_s and B_s are nearly the same near the nose of the magnetosphere for northward and southward IMF. This is particularly true for the high-Mach-number pair (bottom panel). For the high-Mach-number pair of simulations, the difference in magnetic field values over the average value $\Delta B/\langle B\rangle$ is about 1% and likewise the difference in number-density values over the average value $\Delta n/\langle n\rangle$ is about 1%; for the low-Mach-number pair of simulations, the difference in magnetic field values over the average value $\Delta B/\langle B\rangle$ is about 15% and $\Delta n/\langle n\rangle$ is about 29%. This is evidence that the dayside reconnection does not strongly affect the values of ρ_s and B_s near the nose of the magnetosphere, at least for the parameters examined here. Since the presence of reconnection does not strongly alter the values of ρ_s and B_s, reconnection does not significantly change the flow pattern of the magnetosheath around the Earth. In a similar fashion the magnetic field strength B and the plasma density n are plotted in the magnetosphere out to the magnetopause in the two panels of Figure 12 for northward-IMF and southward-IMF conditions. The top panel is at low Mach number and the bottom panel is at high Mach number. As can be seen in the two panels, the magnetic field strength B_m differs very little at the magnetopause between northward- versus southward-IMF cases. Hence reconnection does not affect the value of B_m. As can be seen in the top panel of Figure 12, the rate of reconnection can affect the value of ρ_m at the magnetopause; this is will be elaborated upon further in Section V. As demonstrated by Figures 11 and 12, reconnection itself does not modify the parameters (B_m, B_s, and ρ_s) going into the right-hand side of expression (4). (The parameter ρ_m may vary, but it is usually too small to have an effect in expression (4).) Hence Scenario 1 (where reconnection alters the local plasma parameters to produce a balance) does not occur. In that sense, dayside reconnection is not "driven" [cf. *Axford*, 1984; *Sato and Hayashi*, 1979; *Birn et al.*, 2005] by the solar wind. Rather the magnetosheath plasma flows around the magnetosphere and some of the magnetic flux in the flow is captured by reconnection. The flow around happens whether or not reconnection goes on. The parameters of the solar wind, in part, control how much reconnection occurs.

5. Plasmasphere Effect

[27] The fact that during geomagnetic storms, very high density plasma from the inner magnetosphere can convect into the dayside reconnection site was the motivation for the present reconnection-rate study. It was hypothesized [*Borovsky and Steinberg*, 2006] that this high-density plasma could mass load dayside reconnection by reducing the local Alfven speeds, and reductions in the amount of solar wind/magnetosphere coupling during such times were subsequently detected [*Borovsky and Denton*, 2006]. The Cassak-Shay relation (1) and (2) confirmed here to hold at the dayside reconnection site lends theoretical support to this notion [see also *Borovsky and Hesse*, 2007].

[28] A demonstration of the plasmaspheric effect occurs in Simulation B (see Figure 8) when high-density magnetospheric plasma chokes the rate of reconnection beginning at about t = 150 min. In this simulation, ionospheric outgassing from the r = 2.5 R_E inner boundary builds up a high-density plasma in the inner magnetosphere. As the solar wind velocity increases with time in the simulation (see t = 90 min to t = 150 min in the bottom panel of Figure 7), the reconnection rate increases (see t = 90 to t = 150 in the bottom panel of Figure 8). As magnetospheric convection strengthens (since the rate of dayside reconnec-

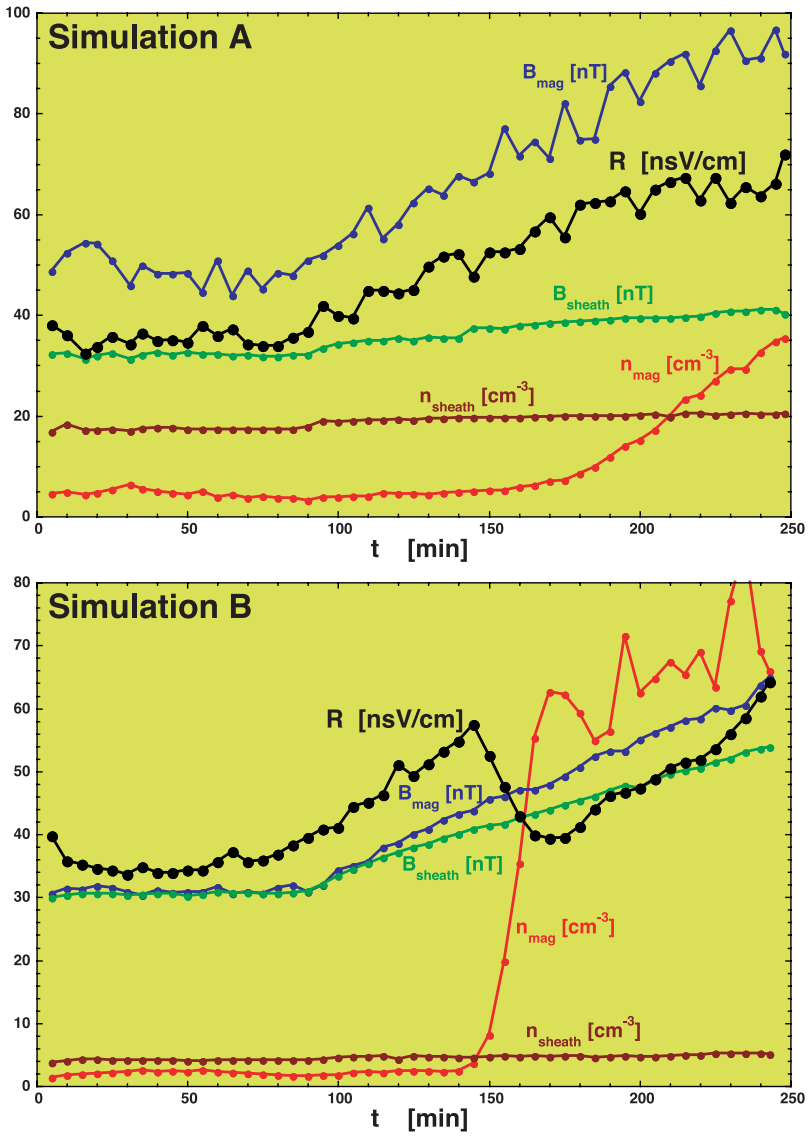

Figure 8. For Simulation A (top) and Simulation B (bottom), the four local plasma parameters B_s (green), B_m (blue), ρ_s (dark red), and ρ_m (red) and the measured reconnection rate at the nose (black) are plotted as functions of time every 5 min.

tion R is steadily increasing) magnetospheric convection eventually pulls out this high-density plasma, forming a "plume" that flows to the dayside neutral line. This plume occurrence in the simulation was unplanned, but very fortuitous. (A note of caution for the reader: the cold plasma in the simulation is by no means a proper plasmasphere, which would be build up from field-aligned ionospheric outgassing at all latitudes into a corotating inner magnetosphere.) In Figure 13 this plume is shown in the equatorial plane of the simulation. Note that the high-density material only flows into a narrow region around the nose of the magnetosphere. In Figure 14 the dayside reconnection rate R is plotted as a function of Y across the front of the magnetosphere at two instants of time from Simulation B. The mass density of the magnetospheric plasma flowing into the reconnection line is also plotted as a function of Y across the front of the magnetosphere. The top panel of Figure 14 corresponds to a time just prior to the high-density plume and the bottom panel corresponds to a time when the plume is ongoing. As can be seen in the bottom panel, the localized high-density magnetospheric plasma locally reduces the reconnection rate. This effect amounts to a mass loading of the reconnection process, resulting in a significant reduction of the reconnection rate. As can be seen in the bottom panel of Figure 8 by extrapolating the upward trend of the reconnection-rate curve (black) beyond t = 150 min and comparing that extrapolation with the reduced curve, the reconnection rate is reduced by about a factor of 2 by the high-density magnetospheric plasma. In the bottom panel of Figure 14, making extrapolations of the reconnection-rate curve in Y across the nose of the magnetosphere and comparing with the reduced curve at the nose yields a similar conclusion: that the plasmaspheric effect reduced the reconnection rate by about a factor of 2 for the parameters of this simulation.

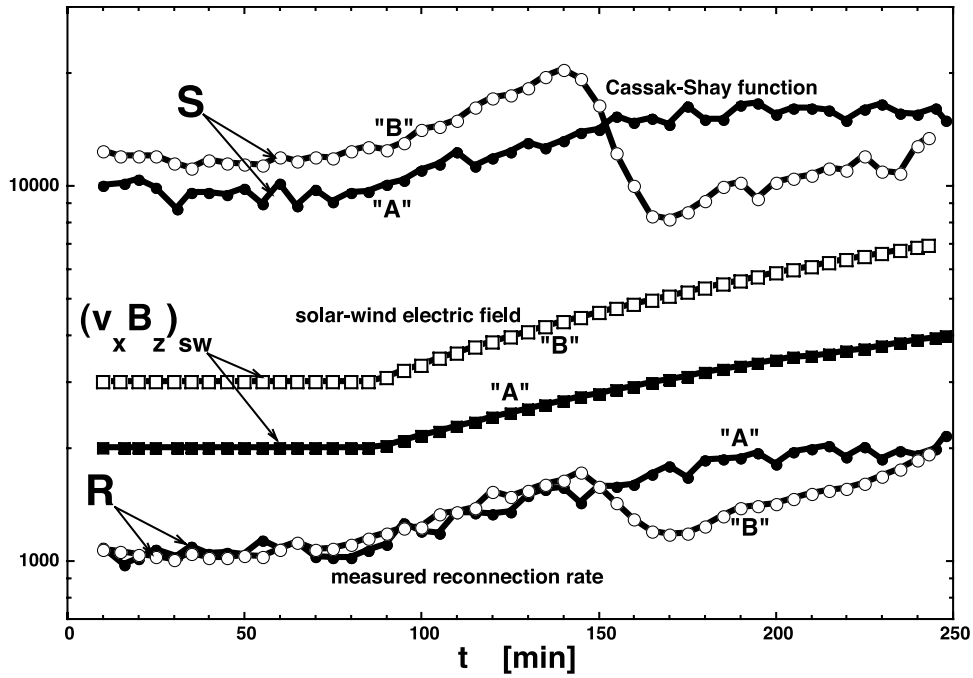

Figure 9. For Simulation A (solid points) and Simulation B (hollow points), the measured reconnection rate R at the nose, the solar wind electric field $(v_xB_z)_{sw}$, and the Cassak-Shay function S (expression (2) evaluated with measured values of B_s, B_m, ρ_s, and ρ_m) are plotted as functions of time every 5 min.

[29] The dayside magnetosphere in the absence of a plasmaspheric drainage plume can have a plasma number density as low as 0.5 cm^{-3}, whereas a plume can have a plasma number density of over 100 cm^{-3} [*Borovsky and Denton*, 2006]. Further, the oxygen and helium content of a drainage plume can give it an effective ionic mass of ~2.5 amu. One can see from an inspection of expressions (1) and (2) that a change of the magnetospheric plasma density n_m from n_m = 0.5 cm^{-3} (low-density dayside magnetosphere) to n_m = 100 cm^{-3} (plasmaspheric drainage

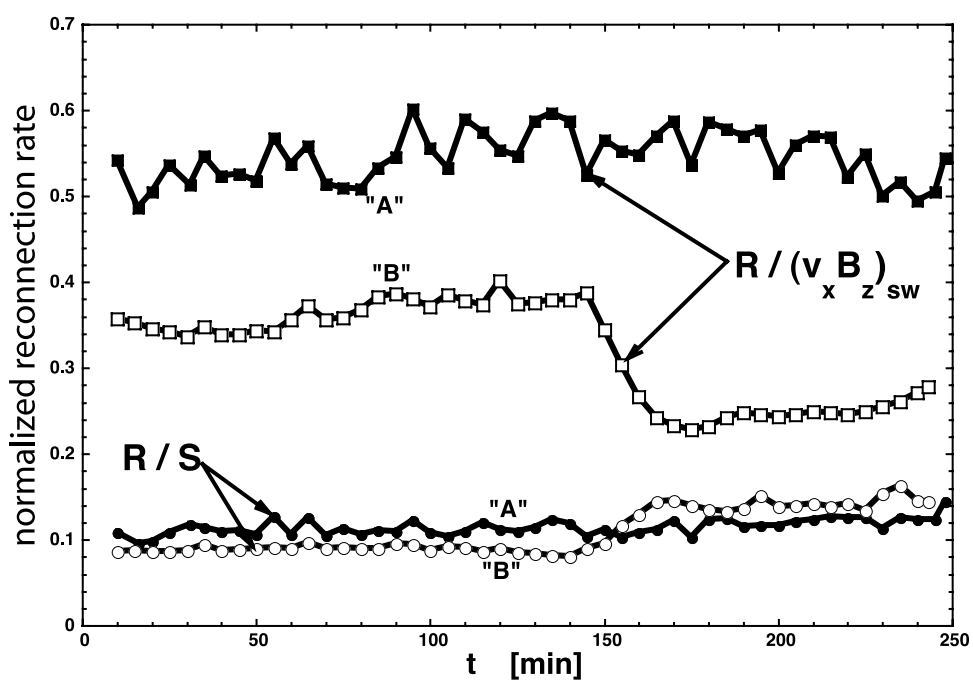

Figure 10. For Simulation A (solid points) and Simulation B (hollow points), the ratio of the measured reconnection rate R at the nose to the solar wind electric field $(v_xB_z)_{sw}$, and the ratio of the measured reconnection rate R at the nose to the Cassak-Shay function S (expression (2) evaluated with measured values of B_s, B_m, ρ_s, and ρ_m) are plotted as functions of time every 5 min.

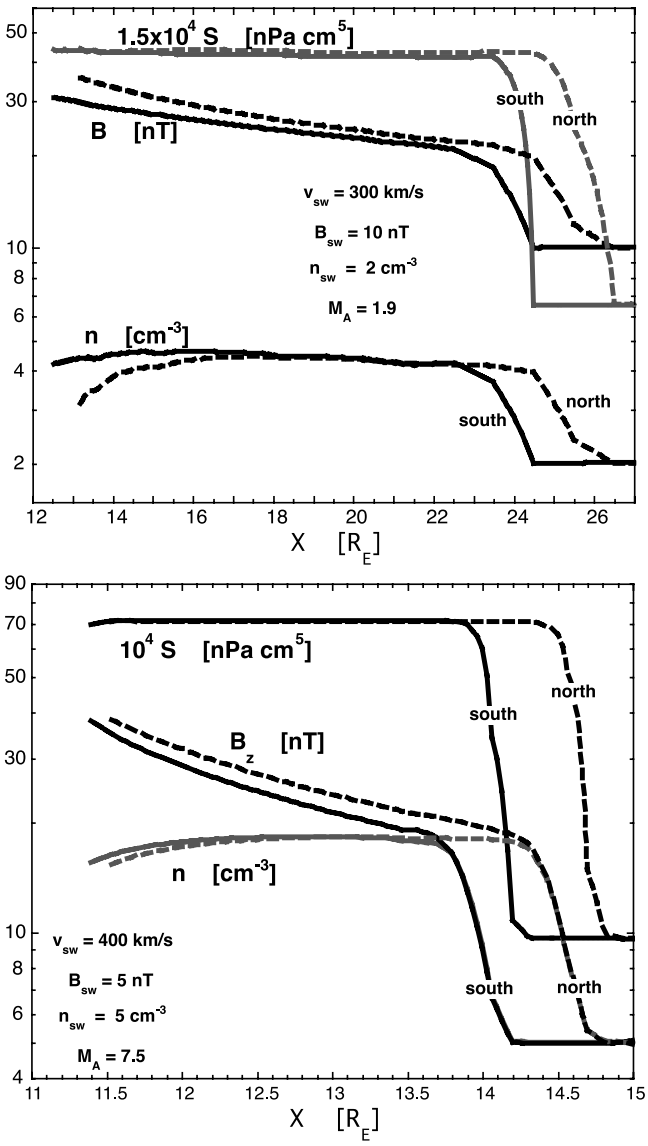

Figure 11. Magnetosheath X profiles of critical plasma parameters are compared between northward-IMF (dashed curves) and southward-IMF (solid curves) simulations. In the top is a pair of low-Mach-number simulations: Simulation B at t = 1:25 (southward) and an identical simulation with northward IMF. In the bottom is a pair of high-Mach-number simulations from the CCMC library (ESS261_CCMC_031307_3 courtesy of Ray Walker); this pair uses the high-resolution grid as in Simulation A, but the southward-IMF simulation does not have a resistive spot. Instead reconnection occurs via numerical effects.

plume) may substantially alter the reconnection rate at the dayside magnetopause where the plume plasma flows into it. Using the results of the present study, the plasmaspheric effect will be pursued further in a future study.

[30] Note that there is another potentially stronger effect. During geomagnetic storms auroral outflows of cool oxygen ions and the subsequent convection of plasma from the nightside to the dayside can result in high mass densities throughout the dayside magnetosphere. These high-density auroral plasmas might mass load the entire dayside reconnection line.

6. Summary and Discussion

6.1. Summary

[31] Using the BATSRUS simulation code at the CCMC, three-dimensional high-resolution MHD simulations with a resistive spot on the magnetopause were run for a large range of solar wind Mach numbers. Idealized solar wind

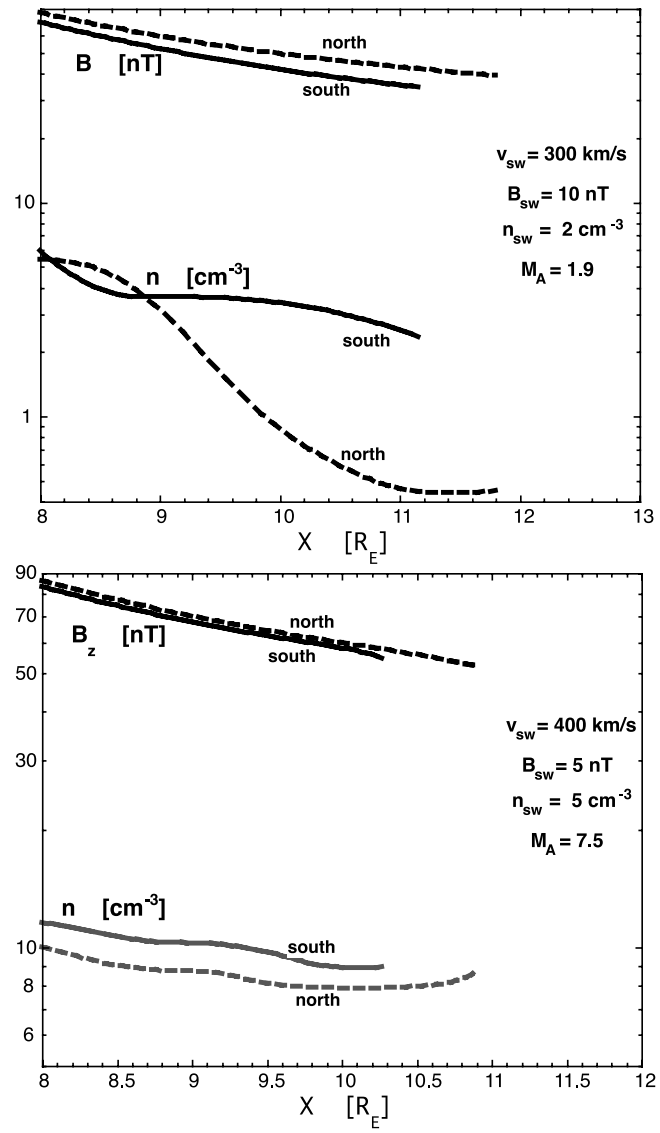

Figure 12. Magnetospheric X profiles of critical plasma parameters are compared between northward-IMF (dashed curves) and southward-IMF (solid curves) simulations. In the top is a pair of low-Mach-number simulations: Simulation B at t = 1:25 (southward) and an identical simulation with northward IMF. In the bottom is a pair of high-Mach-number simulations from the CCMC library (ESS261_CCMC_031307_3 courtesy of Ray Walker); this pair uses the high-resolution grid as in Simulation A, but the southward-IMF simulation does not have a resistive spot. Instead reconnection occurs via numerical effects.

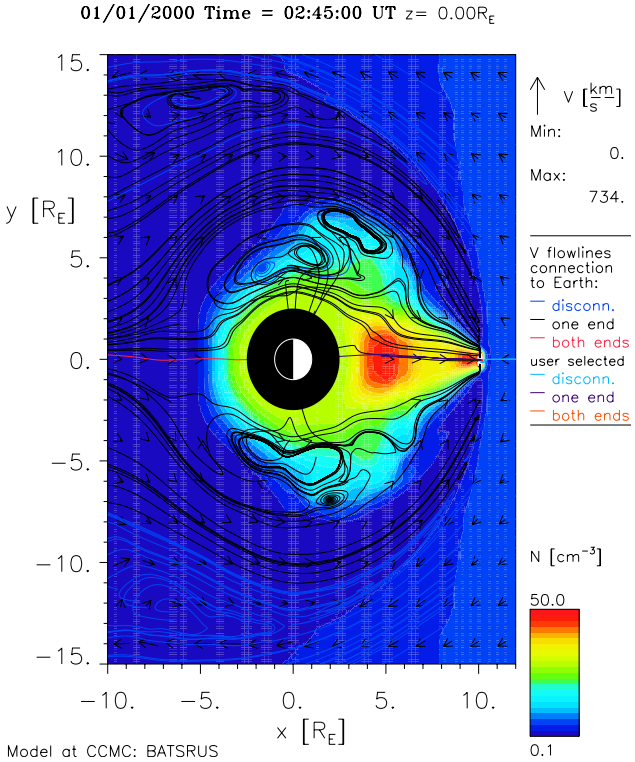

Figure 13. Plasma number density is shown (color) in the equatorial plane at a time in Simulation B when a high-density plume of magnetospheric plasma is flowing into the reconnection site at the nose of the magnetosphere. Flow streamlines are indicated.

parameters and southward IMF were used. The rate of magnetic field-line reconnection at the nose of the magnetosphere was measured, upstream solar wind parameters were recorded, and local plasma parameters near the reconnection site were measured. The primary findings are the following.

[32] 1. Strong variations in the reconnection rate were observed in association with variations in local plasma parameters, but no corresponding variations in upstream-solar wind parameters.

[33] 2. The Cassak-Shay formula for the reconnection rate between asymmetric plasmas was evaluated and found to describe the rate of reconnection at the dayside magnetopause. According to this formula, reconnection is a local phenomena and the rate of reconnection is controlled by the plasma parameters at the reconnection site.

[34] 3. The four plasma parameters that control dayside reconnection are B_s (the magnetic field strength in the magnetosheath near the reconnection site), B_m (the magnetic field strength in the magnetosphere near the reconnection site), ρ_s (the plasma mass density in the magnetosheath near the reconnection site), and ρ_m (the plasma mass density in the magnetosphere near the reconnection site). It is also anticipated that the IMF clock angle θ will play a role in the reconnection rate.

[35] 4. It was argued that the dayside reconnection does not significantly alter the magnetosheath flow pattern, so reconnection should not significantly alter the four local parameters that control the reconnection rate. If this is true then it disallows the scenario wherein reconnection is "driven" by the solar wind and the local plasma parameters change to adjust the reconnection rate to balance the driving.

[36] 5. Northward-IMF simulations were compared with southward-IMF simulations at both high and low Mach numbers. It was found that the critical plasma parameters B_s, B_m, and ρ_s did not significantly vary between southward IMF (reconnection on) and northward IMF (reconnection off).

[37] 6. The "plasmasphere effect" was observed in the simulations, wherein high-density magnetospheric plasma flows into the dayside reconnection site and mass loads the reconnection. A spatially localized plume of plasma was observed to locally reduce the reconnection rate at the magnetopause. The plasmasphere effect is described by the Cassak-Shay formula.

[38] 7. The major conclusion is that reconnection is a local phenomenon, controlled by local plasma parameters. It is not driven by the solar wind electric field, although the solar wind largely controls its rate. The magnetosphere

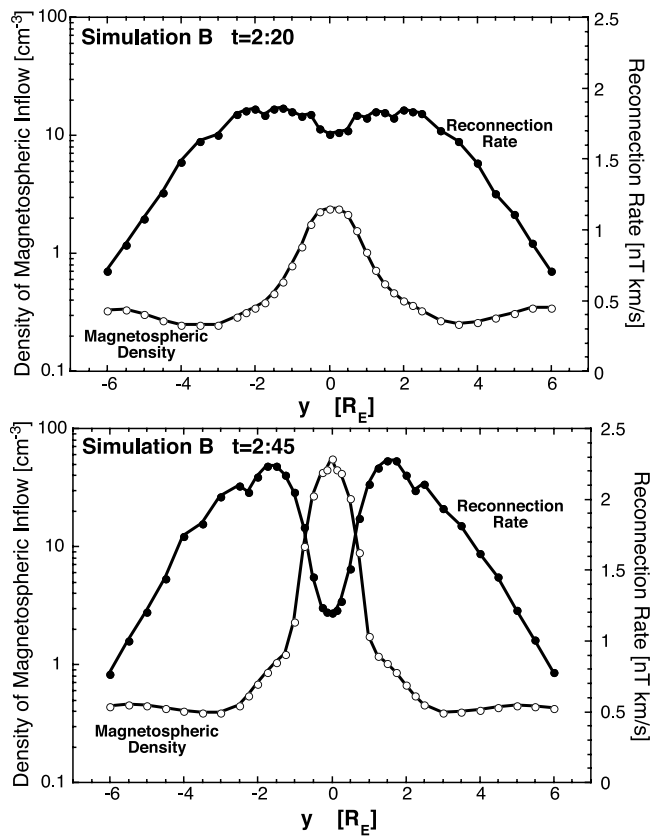

Figure 14. For two times in Simulation B, the measured reconnection rate (solid points) and the magnetospheric plasma density (hollow points) are plotted as a function of Y across the dayside magnetosphere. The top pertains to a time just before a high-density plume of high-density magnetospheric plasma flows into the reconnection site at the nose and the bottom panel pertains to a time when a high-density plume is flowing into the reconnection site at the nose.

exerts some control of the reconnection rate through the magnetospheric-plasma mass density.

6.2. Local Control of Dayside Reconnection

[39] Reconnection is a local process; the rate of reconnection is determined/controlled by the local plasma properties. At the dayside magnetopause reconnection takes place between the magnetospheric plasma and the magnetosheath plasma. The rate of reconnection is controlled by the parameters of these two plasmas near the magnetopause These plasma parameters are controlled, in turn, by the parameters of the solar wind, by the manner in which the bow shock modifies the solar wind, and by the properties of the magnetosheath flow pattern, and by the density of the dayside magnetosphere.

[40] Note that the electric field E of the solar wind is not the direct driver of dayside reconnection. It is often stated that the y component E_y of the solar wind electric field controls the reconnection rate at the magnetopause neutral line [e.g., *Siscoe and Crooker*, 1974; *Wygant et al.*, 1983; *Freeman and Farrugia*, 1999], and several theoretical [*Gonzalez and Mozer*, 1974; *Siscoe and Crooker*, 1974; *Kan and Lee*, 1979] and empirical [*Burton et al.*, 1975; *Gonzalez and Gonzalez*, 1984; *Lei et al.*, 1981; *Wygant et al.*, 1983] pictures of solar wind/magnetosphere coupling are based on the solar wind electric field. According to the findings of the present report, the solar wind electric field $\mathbf{E} = -\mathbf{v} \times \mathbf{B}$ is at best an indirect driver: indirect in that v and B of the solar wind in part determine the relevant local plasma parameters at the magnetopause.

[41] The plasmasphere effect is the reduction of dayside reconnection caused by high-density plasmaspheric plasma flowing into the reconnection site. If dayside reconnection is "driven", then the local plasma parameters adjust so that the reconnection rate goes at the driving rate. In that case there would be no plasmasphere effect: instead the local parameters would adjust to overcome the effect of high-density magnetospheric plasma. As can be seen at time t > 150 min in the bottom panel of Figure 8, high-density magnetospheric plasma does reduce the rate of reconnection; this is strong/further evidence that dayside reconnection is not "driven".

[42] Dayside-reconnection control by the local plasma parameters presents a more-physical way of thinking about solar wind/magnetospheric coupling and presents a new methodology for calculating, from first principles, solar wind/magnetospheric coupling. This method is pursued in a follow-on report [*Borovsky*, 2008].

6.3. Plasma Pileup at the Nose of the Magnetosphere

[43] The pileup of plasma in the flow pattern near a reconnection site has been considered often [e.g., *Parker*, 1973b; *Sonnerup and Priest*, 1975; *Litvinenko et al.*, 1996; *Craig and Watson*, 2000; *Dorelli and Birn*, 2003; *Dorelli et al.*, 2004; *Sullivan et al.*, 2005]. Pileup at the magnetopause associated with reconnection is not seen in the global-MHD simulations of this report.

[44] A pileup argument concerning driven reconnection could be made thus: *vB_z away from the reconnection site is the driver function for reconnection and plasma will pile up until the reconnection rate (set by the local plasma parameters) matches the vB_z driver.* That argument should work in a two-dimensional geometry, but in the three-dimensional situation at the nose of the magnetosphere flow around the magnetosphere dominates over the reconnection rate, making pileup irrelevant to the reconnection rate.

[45] When northward-IMF (reconnection-off) simulations are compared with southward-IMF (reconnection-on) simulations, very little difference is seen in the local plasma parameters B_m, B_s, ρ_m, and ρ_s that govern reconnection at the nose. Two such pairs of simulations are shown in Figures 11 and 12; in the top panel a high-Mach-number pair is shown and in the bottom panel a low-Mach-number pair is shown. Since the plasma parameters are nearly the same for reconnection off and reconnection on, there is no pileup associated wit the reconnection rate. There is pileup of plasma on the magnetospheric obstacle, but it is not reconnection related.

6.4. Errors in Simulating and Measuring Dayside Reconnection

[46] There are three identifiable errors in our evaluation of the Cassak-Shay formula for determining the reconnection rate at the dayside magnetosphere. The first two concern the analysis of the MHD simulations and the third concerns the accuracy of the simulations.

[47] First, in the vicinity of the reconnection site there are very steep gradients in X of the four local plasma parameters B_s, B_s, ρ_s, and ρ_m. Slight displacements in the determination of the edges of the magnetospheric and magnetosheath plasmas (determined by changes in the functional behavior of the plasma parameters) can lead to large changes in the values of the four parameters used to evaluate the Cassak-Shay formula. As can be seen in Figure 8, such errors lead to ~5% fluctuations in the measured values of the plasma parameters. Hopefully, there are no systematic errors.

[48] Second, at the nose of the magnetosphere there are three-dimensional flow patterns. The flow streamlines in the equatorial plane converge toward the nose in the magnetosphere and diverge away from the nose in the magnetosheath (see Figure 4). Because of these nonplanar flows, the values of B and ρ just outside of the reconnection site (where they are chosen for the Cassak-Shay formula) can differ from the values closer to the reconnection site.

[49] Third, a physical resistivity is added to the nose of the magnetosphere to control the physics of reconnection there, but no equivalent viscosity is added. In the MHD simulations, when gradient scales become comparable to the gridspacing then non-MHD terms become important in the equations that the code actually solves. For simplicity, these "numerical errors" are termed "numerical resistivity" and "numerical viscosity". As discussed in section 2, a physical resistivity was added to the nose of the magnetosphere in these simulations to keep the gradient scales of the magnetic field larger than the gridspacing and to control the physics of the reconnection (at least to control the physics of magnetic diffusion). However, no physical viscosity was added in these simulations. Hence velocity gradients are free to steepen to the gridscale where nonMHD effects can alter the flow. An example of this is shown in Figure 15 where the X-component velocity and the Z-component magnetic field are plotted as a function of X at Y = 1 R_E and Z = 0, along with the resistivity η. As can be seen in the

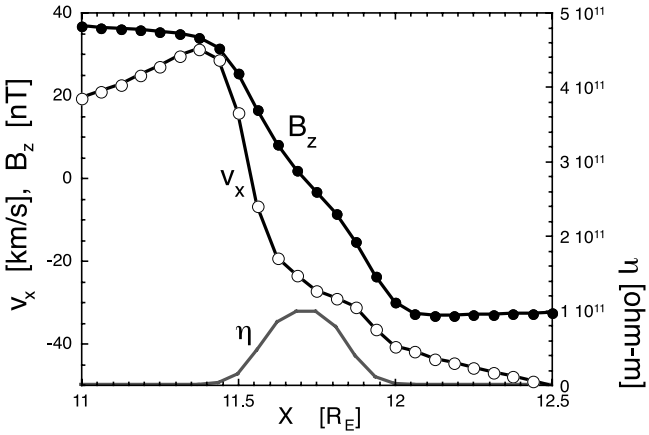

Figure 15. Gradients in v_x and B_z are compared in an X cut at Y = 1 R_E in the equatorial plane. The plotted points are each one gridspace apart. Also plotted (right axis) is the resistivity.

figure, the magnetic field gradient scale corresponds to the width of the resistive spot, but the velocity has a gradient scale that is only a few gridspaces. Because of the numerical errors on the velocity associated with gridscale gradients, the flow pattern near the reconnection site may be in error and plasma transport and magnetic field-line transport may not follow the flow streamlines.

6.5. Future Work

[50] The simulations (A and B) analyzed here both have due-southward IMF, with an IMF "clock angle" θ of 180°. Also, the simulations do not have a tilt to the magnetic dipole relative to the Sun-Earth line. In future, an analysis of the reconnection rate as a function of θ needs to be made. This study will be difficult because the reconnection line will move off the equatorial plane and it will be difficult to track, difficult to position the resistive spot on, and difficult to analyze. Additionally, complicating effects of dipole tilt (again, with off-equatorial reconnection) need to be analyzed.

[51] The Cassak-Shay equation (1) and (2) for the reconnection rate was derived by assuming that reconnection annihilates all of the magnetic field in the inflowing plasma and converts all of this $B^2/8\pi$ energy into ram kinetic energy of the outflowing plasma beams. A more advanced derivation of the reconnection rate that accounts for the energy that goes into plasma heating is needed for improved accuracy.

[52] The finding of this report that the dayside reconnection rate is controlled via local plasma parameters opens a pathway to a new formulation of solar wind/magnetosphere coupling: a physics-based derivation, not an empirical methodology based on the guess that vB_z of the solar wind is related to the dayside reconnection rate). This path is followed in a subsequent manuscript [*Borovsky*, 2008].

Appendix A: Requirements for the Resistive Spot

[53] The GEM Reconnection Challenge [*Birn et al.*, 2001] concluded that, in the regime of fast reconnection, reconnection rates do not depend on the mechanism that breaks the frozen-in condition (i.e., kinetic plasma effects or resistivity), just so that it is broken. Further, the GEM Challenge demonstrated that MHD simulations can get the correct reconnection rate if they properly emulate the breaking of the frozen-in condition in a diffusion zone. This proper emulation occurs if resistivity is added that is (1) localized and (2) strong. The questions arise: How localized and how strong?

[54] The question of how strong the resistivity should be is answered as follows. For plasma flowing across the resistive spot, the resistivity must be strong enough for the magnetic field to be able to diffuse out of the plasma as it crosses the spot. Hence the magnetic diffusion time τ_{diff} must be shorter than the convection time τ_{conv}. In Figure A1 the streamlines (black curves) for plasma crossing the spot (gray region) at the reconnection site is sketched. To the right of the spot would be the inflowing magnetopause plasma and to the left would be the inflowing magnetospheric plasma, toward the top and the bottom is the outflowing reconnected plasma. One example flow line through the spot is highlighted as the thick black curve. The plasma flows in (from the left) at about 0.1 v_A and it flows out (toward the top) at about v_A, where v_A is the Alfven speed measured in the inflowing plasma away from the spot. The spot has a halfwidth of L_x in the X direction (horizontal) and a halfwidth of L_y in the Y direction

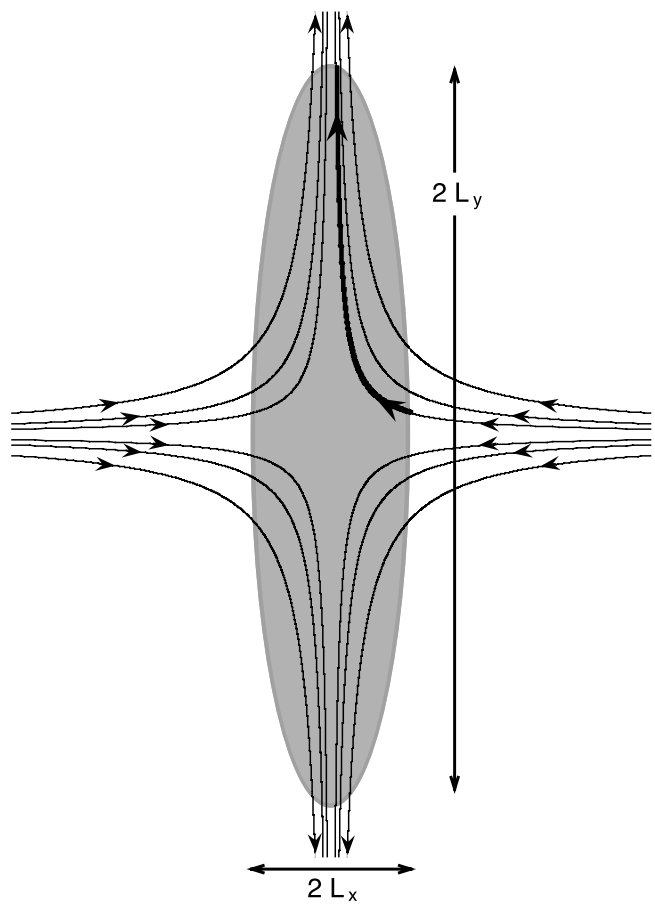

Figure A1. A sketch of the plasma flow through the resistive spot (gray shading) at the dayside reconnection site in the MHD simulations.

(vertical). Hence the convection time is $\tau_{conv} \approx 10\ L_x/v_A + L_y/v_A$. If $L_y \approx 10\ L_x$, then this becomes $\tau_{conv} \approx 20\ L_x/v_A$. For magnetic field gradients in the X direction, the magnetic diffusion time (in MKS units) is $\tau_{diff} \approx (\mu_o/\eta)L_x^2$. Requiring $\tau_{diff} < \tau_{conv}$ yields

$$\mathrm{Lu} \equiv v_A L_x \mu_o/\eta < 20 \tag{A1}$$

where Lu is the Lundqvist number [e.g., *Cowling*, 1976] (a magnetic Reynolds number with a flow speed related to an Alfven speed) for the plasma flow through the resistive spot. The Lundqvist-number criteria of expression (A1) specifies how strong the resistivity must be for a given spot size L_x. This could explicitly be written as $\eta > v_A L_x \mu_o/20$. *Birn et al.* [2008] parametrically studied the reconnection rate versus the strength of the resistivity in resistive spots: providing that the resistivity η is large enough, the reconnection rate is independent of the actual value of η.

[55] The second question (how localized?) can be rephrased: How big should the spot be? The answer is: The spot should be at least several gridspacings wide. The reason is as follows. In ideal-MHD simulations gradients will steepen until they are limited by the gridspacing. When a gradient has a scale thickness that is comparable to the gridspacing, then large numerical terms associated with the finite difference scheme enter the MHD equations. At a steep gradient MHD is not being solved in the simulation; something else describes the evolution of the plasma. At these gradients numerical errors dominate the solution. If this were to happen at the reconnection site, then the reconnection rate would not be self-consistently by MHD. When a resistive spot is used, the gradients in the magnetic field are diffused to the spot width 2 L_x. So, in order to keep the magnetic field gradients from steepening to the gridspacing at the reconnection site, the resistive spot must have a width 2 L_x that is at least a few gridspaces wide.

[56] Of course, a small spot is desirable. However to use a smaller and smaller spot, a finer and finer gridspacing Δ must be used. As stated in section 2, the simulations of this report have Δ = 1/16 R_E and L_X = 1/8 R_E, so that 2 L_X = 4Δ.

[57] With L_x = 1/8 R_E and $\eta = 1.26 \times 10^5$ ohm-m, the simulations of this report have a Lundqvist number Lu = 1.3 at the reconnection site, which is considerably less than 20, as required.

[58] The resistivity of the spot is about an order of magnitude higher than the numerical resistivity observed in the code without the resistive spot (determined at a gridspacing of Δ = 1/16 R_E to be 2×10^4 ohm-m by comparing the E_y electric field outside of the magnetopause with the j_y current density in the magnetopause and taking $\eta_{numerical} = E_y/j_y$).

[59] For identical simulations with and without the resistive spot, the measured reconnection rates are higher when a resistive spot is used than when no spot is used (and in which case reconnection is enable via numerical error at steep gradients). When a spot is used, the reconnection site favors the location of the spot. When no spot is used, the reconnection site favors the locations of boundaries between grid blocks (i.e., the reconnection site is collocated upon sites where the resolution of the numerical grid changes).

[60] **Acknowledgments.** The authors wish to thank Paul Cassak, Anna Chulaki, Benoit Lavraud, Jimmy Raeder, Lutz Rastaetter, and Mike Shay for their help and for helpful conversations. Joe Borovsky and Joachim Birn would also like to acknowledge the CCMC at NASA/Goddard Space Flight Center for their hospitality. All simulations were performed using the CCMC at NASA/GSFC. This work was supported by the NSF National Space Weather Program (at Los Alamos) and by the NASA Heliospheric Theory Program (at Los Alamos and at NASA/Goddard).

[61] Amitava Bhattacharjee thanks David Sibeck and another reviewer for their assistance in evaluating this paper.

References

Anderson, B. J., and S. A. Fuselier (1993), Magnetic pulsations from 0.1 to 4.0 Hz and associated plasma properties in the Earth's subsolar magnetosheath and plasma depletion layer, *J. Geophys. Res.*, *98*, 1461.

Axford, W. I. (1984), Driven and non-driven reconnection: Boundary conditions, in *Magnetic Reconnection in Space and Laboratory Plasmas*, edited by E. W. Hones, p. 360, AGU, Washington, D. C.

Birn, J., and M. Hesse (2001), Geospace Environment Modeling (GEM) magnetic reconnection challenge: Resistive tearing, anisotropic pressure and Hall effects, *J. Geophys. Res.*, *106*, 3737.

Birn, J., and E. R. Priest (Eds.) (2007), *Reconnection of Magnetic Fields*, Sects. 2.1 and 4.2.4, Cambridge Univ. Press, New York.

Birn, J., et al. (2001), Geospace Environment Modeling (GEM) magnetic reconnection challenge, *J. Geophys. Res.*, *106*, 3715.

Birn, J., et al. (2005), Forced magnetic reconnection, *Geophys. Res. Lett.*, *32*, L06105, doi:10.1029/2004GL022058.

Birn, J., J. E. Borovsky, and M. Hesse (2008), Properties of asymmetric magnetic reconnection, *Phys. Plasmas*, *15*, 032101.

Borovsky, J. E. (2008), The rudiments of a theory of solar-wind/magnetosphere coupling derived from first principles, *J. Geophys. Res.*, doi:10.1029/2007JA012646, in press.

Borovsky, J. E., and M. H. Denton (2006), The effect of plasmaspheric drainage plumes on solar-wind/magnetosphere coupling, *Geophys. Res. Lett.*, *33*, L20101, doi:10.1029/2006GL026519.

Borovsky, J. E., and M. Hesse (2007), The reconnection of magnetic fields between plasmas with different densities: Scaling relations, *Phys. Plasmas*, *14*, 102,309.

Borovsky, J. E., and J. T. Steinberg (2006), The "calm before the storm" in CIR/magnetosphere interactions: Occurrence statistics, solar-wind statistics, and magnetospheric preconditioning, *J. Geophys. Res.*, *111*, A07S10, doi:10.1029/2005JA011397.

Burton, R. K., R. L. McPherron, and C. T. Russell (1975), An empirical relationship between interplanetary conditions and Dst, *J. Geophys. Res.*, *80*, 4204.

Cassak, P. A., and M. A. Shay (2007), Scaling of asymmetric magnetic reconnection in collisional plasmas, *Phys. Plasmas*, *14*, 102144.

Cowley, S. W. H., et al. (2003), Solar-wind-magnetosphere-ionosphere interactions in the Earth's plasma environment, *Philos. Trans. R. Soc. Ser. A*, *361*, 113.

Cowling, T. G. (1976), *Magnetohydrodynamics*, Sect. 2.1, Adam Higler, London.

Craig, I. J. D., and P. G. Watson (2000), Flare-like energy release by flux pile-up reconnection, *Solar Phys.*, *191*, 359.

De Zeeuw, D. L., T. I. Gombosi, C. P. T. Groth, K. G. Powell, and Q. F. Stout (2000), An adaptive MHD method for global space weather simulations, *IEEE Trans. Plasma Sci.*, *28*, 956.

Dorelli, J. C., and J. Birn (2003), Whistler-mediated magnetic reconnection in large systems: Magnetic flux pileup and the formation of thin current sheets, *J. Geophys. Res.*, *108*(A3), 1133, doi:10.1029/2001JA009180.

Dorelli, J. C., M. Hesse, M. M. Kuznetosva, L. Rastaetter, and J. Raeder (2004), A new look at driven magnetic reconnection at the terrestrial subolar magnetopause, *J. Geophys. Res.*, *109*, A12216, doi:10.1029/2004JA010458.

Dungey, J. W. (1961), Interplanetary magnetic field and the auroral zones, *Phys. Rev. Lett.*, *6*, 47.

Freeman, M. P., and C. J. Farrugia (1999), Solar wind input between substorm onsets during and after the October 18–20, 1995, magnetic cloud, *J. Geophys. Res.*, *104*, 22,729.

Goertz, C. K., L.-H. Shan, and R. A. Smith (1993), Prediction of geomagnetic activity, *J. Geophys. Res.*, *98*, 7673.

Gombosi, T. I., D. L. De Zeeuw, C. P. T. Groth, and K. G. Powell (2000), Magnetospheric configuration for Parker-spiral IMF conditions: Results of a 3D AMR MHD simulation, *Adv. Space Res.*, *26*, 139.

Gonzalez, W. D., and A. L. C. Gonzalez (1984), Energy transfer by magnetopause reconnection and the substorm parameter ε, *Planet. Space Sci.*, *32*, 1007.

Gonzalez, W. D., and F. S. Mozer (1974), A quantitative model for the potential resulting from reconnection with an arbitrary interplanetary magnetic field, *J. Geophys. Res.*, *79*, 4186.
Hesse, M., J. Birn, and M. Kuznetosova (2001), Collisionless magnetic reconnection: Electron processes and transport modeling, *J. Geophys. Res.*, *106*, 3721.
Hones, E. W. (Ed.) (1984), *Magnetic Reconnection in Space and Laboratory Plasmas*, AGU, Washington, D. C.
Huba, J. D. (2005), Hall magnetic reconnection: Guide field dependence, *Phys. Plasmas*, *12*, 012,322.
Huba, J. D., and L. I. Rudakov (2004), Hall magnetic reconnection rate, *Phys. Rev. Lett.*, *93*, 175,003.
Kamide, Y., and J. A. Slavin (Eds.) (1986), *Solar Wind-Magnetosphere Coupling*, Terra Sci., Tokyo.
Kan, J. R., and L. C. Lee (1979), Energy coupling function and solar wind-magnetosphere dynamo, *Geophys. Res. Lett.*, *6*, 577.
Kuznetsova, M. M., M. Hesse, and D. Winske (2001), Collisionless reconnection supported by nongyrotropic pressure effects in hybrid and particle simulations, *J. Geophys. Res.*, *106*, 3799.
Lei, W., R. Gendrin, B. Higel, and J. Berchem (1981), Relationships between the solar wind electric field and the magnetospheric convection electric field, *Geophys. Res. Lett.*, *8*, 1099.
Litvinenko, Y. E., T. G. Forbes, and E. R. Priest (1996), A strong limitation on the rapidity of flux-pile-up reconnection, *Solar Phys.*, *167*, 445.
Otto, A. (2001), Geospace Environment Modeling (GEM) magnetic reconnection challenge: MHD and Hall MHD - Constant and current dependent resistivity models, *J. Geophys. Res.*, *106*, 3751.
Parker, E. N. (1973a), The reconnection rate of magnetic fields, *Astrophys. J.*, *180*, 247.
Parker, E. N. (1973b), Comments on the reconnection rate of magnetic fields, *J. Plasma Phys.*, *9*, 49.
Parker, E. N. (1979), *Comical Magnetic Fields*, Sect. 15.1, Clarendon Press, Oxford.
Petschek, H. E. (1964), Magnetic field annihilation, in *AAS/NASA Symposium on the Physics of Solar Flares*, edited by W. N. Hess, p. 425, NASA SP-50, Washington, D. C.
Phan, T.-D., and G. Paschmann (1995), The magnetosheath region adjacent to the dayside magnetopause, in *Physics of the Magnetopause*, edited by P. Song, B. U. O. Sonnerup, and M. F. Thomsen, p. 115, AGU, Washington, D. C.
Powell, K. G., P. L. Roe, T. J. Linde, T. I. Gombosi, and D. L. De Zeeuw (1999), A solution-adaptive upwind scheme for ideal magnetohydrodynamics, *J. Comput. Phys.*, *154*, 284.
Pritchett, P. L. (2001), Geospace Environment Modeling magnetic reconnection challenge: Simulations with a full particle electromagnetic code, *J. Geophys. Res.*, *106*, 3783.
Pritchett, P. L., and F. V. Coroniti (2004), Three-dimensional collisionless magnetic reconnection in the presence of a guide field, *J. Geophys. Res.*, *109*, A01220, doi:10.1029/2003JA009999.
Raeder, J. (2006), Flux transfer events: 1. Generation mechanisms for strong southward IMF, *Ann. Geophys.*, *24*, 381.
Ridley, A. J., T. I. Gombosi, and D. L. De Zeeuw (2004), Ionospheric control of the magnetosphere: Conductance, *Ann. Geophys.*, *22*, 567.
Rodger, A. S., I. J. Coleman, and M. Pinnock (2000), Some comments on transient and steady-state reconnection at the dayside magnetopause, *Geophys. Res. Lett.*, *27*, 1359.
Russell, C. T. (2000), The solar wind interaction with the Earth's magnetosphere: A tutorial, *IEEE Trans. Plasma Sci.*, *28*, 1818.
Russell, C. T., and G. Atkinson (1973), Comments on a Paper by J. P. Heppner, "Polar cap electric field distributions related to interplanetary magnetic field direction", *J. Geophys. Res.*, *78*, 4001.
Russell, C. T., G. Le, H. Kawano, S. M. Petrinec, and T. L. Zhang (1997), Intrinsic time scale for reconnection on the dayside magnetopause, *Adv. Space Res.*, *19*, 1913.
Sato, T., and T. Hayashi (1979), Externally driven magnetic reconnection and a powerful magnetic energy converter, *Phys. Fluids*, *22*, 1189.
Schindler, K., M. Hesse, and J. Birn (1988), General magnetic reconnection, parallel electric fields, and helicity, *J. Geophys. Res.*, *93*, 5547.
Siscoe, G., and N. Crooker (1974), A theoretical relation between Dst and the solar wind merging electric field, *Geophys. Res. Lett.*, *1*, 17.
Siscoe, G. L., N. U. Crooker, G. M. Erickson, B. U. O. Sonnerup, N. C. Maynard, J. A. Schoendorf, K. D. Siebert, D. R. Weimer, W. W. White, and G. R. Wilson (2002), MHD properties of magnetosheath flow, *Planet. Space Sci.*, *50*, 461.
Shay, M. A., J. F. Drake, B. N. Rogers, and R. E. Denton (1999), The scaling of collisionless, magnetic reconnection for large systems, *Geophys. Res. Lett.*, *26*, 2163.
Shay, M. A., J. F. Drake, B. N. Rogers, and R. E. Denton (2001), Alfvenic collisionless magnetic reconnection and the Hall term, *J. Geophys. Res.*, *106*, 3759.
Song, P., C. T. Russell, J. T. Gosling, M. F. Thomsen, and R. C. Elphic (1990), Observations of the density profile in the magnetosheath near the stagnation streamline, *Geophys. Res. Lett.*, *17*, 2035.
Sonnerup, B. U. O. (1970), Magnetic-field reconnection in a highly conducting incompressible fluid, *J. Plasma. Phys.*, *4*, 161.
Sonnerup, B. U. O. (1974), Magnetopause reconnection rate, *J. Geophys. Res.*, *79*, 1546.
Sonnerup, B. U. O. (1979), Magnetic field reconnection, in *Solar System Plasma Physics*, vol. III, edited by L. T. Lanzerotti, C. F. Kennel, and E. N. Parker, p. 45, Elsevier, New York.
Sonnerup, B. U. O., and E. R. Priest (1975), Resistive MHD stagnation-point flows at a current sheet, *J. Plasma Phys.*, *14*, 283.
Sullivan, B. P., B. N. Rogers, and M. A. Shay (2005), The scaling of forced collisionless reconnection, *Phys. Plasmas*, *12*, 122,312.
Swisdak, M., J. F. Drake, M. A. Shay, and J. G. McIlhargy (2005), Transition from antiparallel to component magnetic reconnection, *J. Geophys. Res.*, *110*, A05210, doi:10.1029/2004JA010748.
Trattner, K. J., S. A. Fuselier, T. K. Yeoman, C. Carlson, W. K. Petersen, A. Korth, H. Reme, J. A. Sauvaud, and N. Dubouloz (2005), Spatial and temporal cusp structures observed by multiple spacecraft and ground based observations, *Surv. Geophys.*, *26*, 281.
Ugai, M., and T. Tsuda (1977), Magnetic field-line reconnection by localized enhancement of resistivity, Part 1, *J. Plasma Phys.*, *17*, 337.
Vasyliunas, V. M. (1984), Steady state aspects of magnetic field line merging, in *Magnetic Reconnection in Space and Laboratory Plasmas*, edited by E. W. Hones, p. 25, AGU, Washington, D. C.
Wang, Y. L., J. Raeder, and C. T. Russell (2004), Plasma depletion layer: Its dependence on solar wind conditions and the Earth dipole tilt, *Ann. Geophys.*, *22*, 4273.
Wu, C. C. (1992), MHD flow past an obstacle: Large-scale flow in the magnetosheath, *Geophys. Res. Lett.*, *19*, 87.
Wygant, J. R., R. B. Torbert, and F. S. Mozer (1983), Comparison of S3-3 polar cap potential drops with the interplanetary magnetic field and models of magnetopause reconnection, *J. Geophys. Res.*, *88*, 5727.
Yan, M., L. C. Lee, and E. R. Priest (1992), Fast magnetic reconnection with small shock angles, *J. Geophys. Res.*, *97*, 8277.
Zwan, B. J., and R. A. Wolf (1976), Depletion of solar wind plasma near a planetary boundary, *J. Geophys. Res.*, *82*, 1636.

J. Birn and J. E. Borovsky, Space Science and Applications Group (ISR-1), Los Alamos National Laboratory, Mail Stop D466, Los Alamos, NM 87545, USA. (jborovsky@lanl.gov)

M. Hesse and M. M. Kuznetsova, Space Weather Laboratory, NASA/Goddard Space Flight Center, Code 674, Greenbelt, MD 20771, USA.